International Journal of Engineering Trends and Technology
ISSN: 2231–5381 / https://doi.org/10.14445/22315381/IJETT-V73I2P103

Volume 73 Issue 2, 22-38, February 2025


*Review Article*

# Investigation of Nanostructured Thin Films Using Scanning Electron Microscopy Technique

Ho Soonmin[1], Ejikeme Ezo Igbokwe[2]

[1]*Faculty of Health and Life Sciences, INTI International University, Negeri Sembilan, Malaysia.*
[2]*Department of Physics with Electronics, Abia State Polytechnic, Aba, Nigeria.*

[1]*Corresponding Author : soonmin.ho@newinti.edu.my*

Received: 20 August 2024 Revised: 14 November 2024 Accepted: 20 January 2025 Published: 21 February 2025

***Abstract*** *- Temperature sensors, optoelectronic devices, laser devices, optical waveguides, and solar cells are just a few applications for thin films. Sputtering, chemical bath deposition, electro deposition, pulsed laser deposition, vacuum evaporation, thermal evaporation, spray pyrolysis, e-beam evaporation, chemical vapor deposition, and spin coating were some of the techniques used to deposit these films. The obtained films could be characterized by means of transmission electron microscopy, Scanning Electron Microscopy (SEM), atomic force microscopy, UV-visible spectroscopy, x-ray photoelectron spectroscopy, x-ray diffraction, Raman spectrometry, Rutherford Backscattering spectrometry, and energy dispersive X-ray analysis. By using a concentrated electron beam to scan the sample surfaces, the SEM technique could create images. These electrons must interact with the atoms (in the produced films), generate various signals, and carry crucial data like composition and surface topography. The specimens could be identified in a variety of settings (high, low, or moist), and the SEM could achieve resolution better than one nanometer. Based on a chosen literature review, the prepared films' morphology was reported in this work. It was demonstrated that the conditions had a significant impact on the grain's size, thickness, and shape. An extended deposition time results in a more pronounced distribution of larger and denser grains that blanket the substrate. It happens because the atoms within the smaller grains possess sufficient energy to diffuse and create a larger grain. Due to this diffusion among grains, leading to a reduction in the boundary between grains and porosity, ultimately yielding a smoother look on the surface of the thin film.*

***Keywords*** *- Thin films, Solar cells, Scanning Electron Microscopy, Morphology, Photovoltaic, Energy efficiency, Energy consumption.*

## 1. Introduction

The growing demand for sustainable energy has driven advancements in solar cell technologies, with thin-film materials playing a pivotal role in this evolution. Thin films offer unique advantages, including lightweight, flexible structures and cost-effectiveness, making them ideal for applications like building-integrated photovoltaics. Their optimized optical and electronic properties enhance energy conversion efficiency, while advanced deposition techniques such as Chemical Vapor Deposition (CVD) improve performance by controlling film morphology [1]. Key materials include amorphous Silicon (a-Si), Cadmium Telluride (CdTe), Copper Indium Gallium Selenide (CIGS), organic films, and perovskites. While a-Si is cost-effective, it suffers from lower efficiency. CdTe and CIGS demonstrate higher efficiencies (22–23%) but face environmental and resource challenges. Perovskite thin films, with efficiencies exceeding 25%, show exceptional promise but require improvements in stability and scalability. Thin films represent a transformative advancement in photovoltaic technology, significantly contributing to sustainable energy solutions [2]. There have been reports of thin-film fabrication using a variety of methods, including sputtering, chemical bath deposition, electro deposition, pulsed laser deposition, vacuum evaporation, thermal evaporation, spray pyrolysis [3], e-beam evaporation, chemical vapor deposition, and spin coating [4]. The prepared films' characterizations were a crucial first step in determining and raising the calibre of the pictures [5]. For example, an irregular structure on the substrate's surface can enhance its contact area with the absorber materials. This can utilize light scattering and impact the efficiency of solar cells. Conversely, it was noted that the effectiveness of the solar cells is significantly influenced by the thin film thickness, and that there is an ideal film thickness that produces the best efficiency outcomes. Common laboratory instruments include transmission electron microscopy [6], photoluminescence spectroscopy, UV-visible spectroscopy, atomic force microscopy, scanning electron microscopy, energy dispersive X-ray analysis, X-ray diffraction [7], Raman spectroscopy technique [8], x-ray

photoelectron spectroscopy, and Rutherford Backscattering spectrometry [9]. Applications for the Scanning Electron Microscope (SEM) exist in the fields of engineering, physical science, and medicine. It uses a concentrated beam of high-energy electrons to generate signals at the surface of the sample [10]. When the electrons in the films interacted with the atoms, they produced signals that revealed crucial details about the crystalline structure, texture, and chemical composition of the films [11]. Data were gathered (in a specific sample area) and two-dimensional (black and white) images were generated. The SEM has many benefits [12], including better resolution, ease of use, speed, the ability to focus multiple samples at once, ease of controlling magnification level, and minimal sample preparation required [13]. One of the main drawbacks of SEM was that it required specialized equipment that needed to be placed in an area free of both electric and magnetic fields. It was also very expensive. It is necessary to perform maintenance and give technicians specialized training [14].

This effort synthesized metal chalcogenide thin films by means of various deposition methods. The process of scanning electron microscopy was used to examine the morphology of the produced films. In this work, metal sulphide, metal telluride, metal oxide and metal selenide films were prepared using different deposition methods. In addition, the morphological of the obtained films will be studied using scanning electron microscopy technique. Finally, it was stated how the experimental setup affected the prepared samples' characteristics based on literature.

## 2. Experimental

To locate research articles published in English related to scanning electron microscopy analysis of thin films, the authors performed a literature review in the pertinent journals from 1997 to 2024. The databases explored included Google Scholar, Taylor & Francis, ACS, Scopus, Wiley Online Library, Science Direct, and MDPI. The terms used included "thin film solar cells", "scanning electron microscopy", "metal sulphide films", "metal oxide films", "metal telluride films", "metal selenide films", "chemical bath deposition", and "physical and chemical deposition methods".

## 3. Literature Survey

### *3.1. SEM Studies of Metal Sulphide Films*

Using the chemical bath deposition method, cadmium sulfide and cadmium zinc sulfide have been deposited onto Fluorine Doped Tin Oxide (FTO) coated glass substrate. Using cadmium sulfate, zinc sulfate, and thiourea, deposition was done at 80 °C with stirring at 200 rpm. According to SEM images [15], the CdS films cover the glass substrate noticeably well and are distributed into smooth, uniform clusters without any creaks (Figure 1(a)). $Zn^{2+}$ was found to form small uniform grains with well-defined grain boundaries in the reaction solution (Figure 1(b)), which may have increased the roughness. As a result, the Zn-incorporated films' effective surface area raised the short-circuit current density values. When comparing CdZnS to CdS, there were significant increases in open-circuit voltage, short-circuit current density, and flat-band voltage of 93 %, 114 %, and 50 %, respectively. Cadmium sulfide has been one of the promising materials. Cadmium sulfide is an II-VI group compound semiconductor with a direct band gap of 2.42 eV at room temperature. Cadmium sulfide exists in two crystalline forms such as hexagonal phase and cubic phase. It is possible to grow CdS films in both phases. Among several methods of CdS thin film deposition, chemical bath deposition is a suitable one. In chemical bath deposition, the structure of the film is influenced by the composition of the bath, temperature and pH of the solution. One of the most common low temperature aqueous techniques for depositing large-area semiconductor thin films is chemical bath deposition, which is also one of the easiest. The chemical bath deposition method produced CdS films that were uniformly adherent and of good quality. The conformally deposited, ultra-thin (less than 50 nm) layers on the substrate surface are one benefit of the CdS layer chemical bath deposition method used in photovoltaic devices.

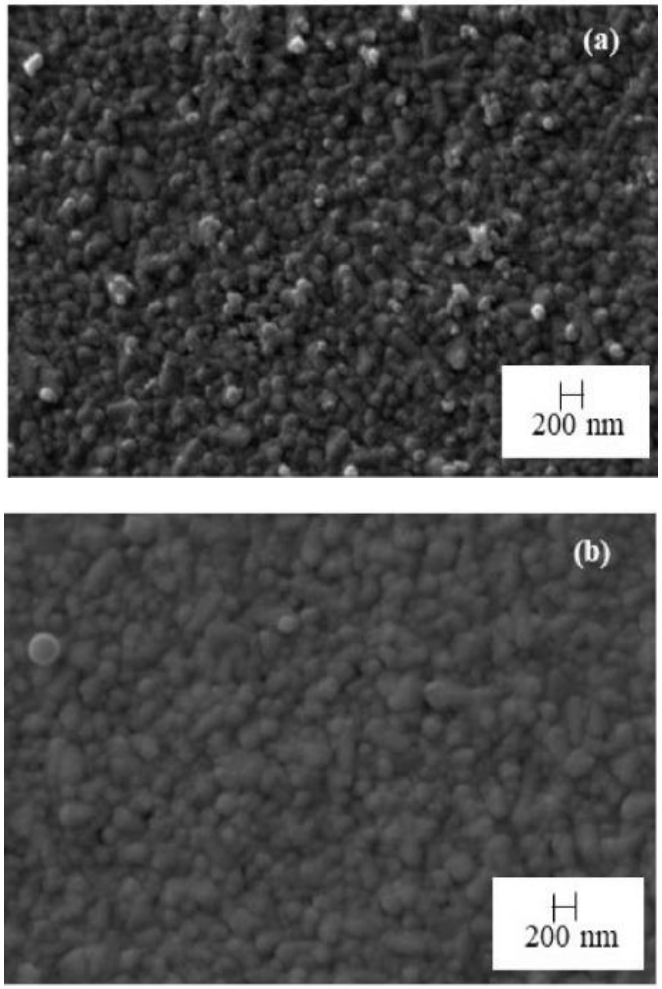


**Fig. 1 SEM images of (a) CdS, and (b) CdZnS films [15]**

Adequate reagents that function as a source of chalcogen ions (thiourea and thioacetamide), a source of metal ions (cadmium chloride) and complexation of the target metal ion are necessary for the chemical bath deposition of cadmium sulfide. Thiourea or thioacetamide hydrolysis reactions in the bath solution provide the sulfur ion. The formation of $Cd(OH)_2$ precipitate on the substrate is not stopped by using a basic bath solution with a pH of approximately 80 ºC (better hydrolysis thiourea), an appropriate complexing agent, and a sufficient concentration of cadmium ions.

The adherent CdS thin film that forms on the substrate in the bath solution is then made possible by this precipitate, which also serves as the matrix. A predominantly homogeneous reaction frequently occurs when the complexing agent concentration is very low [16], resulting in an excess of $Cd(OH)_2$ precipitate in the solution. Additionally, the resulting thin film has poor substrate adherence and grows because of colloids being absorbed. SEM was unable to read the thickness because there was insufficient adhesion to the substrate. The methods of synthesizing $CuInS_2$ thin films can be divided into physical and chemical techniques [17]. Physical methods like sputtering and co-evaporation require very high-vacuum conditions, which enable the growth of phase-pure chalcopyrite crystals with minimal impurities. Sputtering, a typical method for producing $CuInS_2$ under vacuum conditions, involves the sequential deposition of copper (Cu) and indium (In) on substrates, which are then converted into $CuInS_2$ through sulfurization. This approach can generate thin films with excellent uniformity and easily controllable stoichiometries. However, the specific vacuum conditions result in a significantly high cost of thin-film fabrication.

Consequently, researchers are exploring wet chemical methods as an alternative strategy for synthesizing $CuInS_2$. $CuInS_2$ can also be prepared economically and on a large scale by employing solution-based techniques. Coating Cu/In precursor ink onto a rotating substrate is known as spin coating. This method allows for easy control of the Cu/In ratio through modification of the precursor solution's composition. Additionally, repeat spin coating can be used to regulate the thin-film thickness. Large-area film preparation is made easier by spray pyrolysis, which is spraying a precursor solution onto a substrate heated to a high temperature. Here, the concentration of the spray solution can be used to change the $CuInS_2$ composition.

For PEC hydrogen evolution, $CuInS_2$ photocathodes are primarily synthesized via electrodeposition–sulfurization. In this case, conductive substrates are electrochemically coated with copper (Cu) and indium (In) using an electrolytic solution. Cu–In alloy films have also been created via co-deposition. In specific electrolytic baths (Cu-In-S), three elements can be electrodeposited simultaneously. $CuInS_2$ prepared by electrodeposition shows comparable or even better performance than $CuInS_2$ photoelectrodes prepared by co-evaporation or sputtering, in contrast to other chalcopyrite materials. Consequently, a promising method for creating high-performance $CuInS_2$ thin films is electrodeposition. Using the chemical bath deposition method, thin films of $CuZnS_2$ were deposited onto glass substrate both with and without EDTA as complexing agents [18]. The glass slides that had been cleaned and degreased were arranged vertically within the beaker that held the solutions of copper, zinc, and sodium sulfate.

After that, the beaker was left alone for the deposition process for roughly two hours. The time it takes for the copper and zinc ions to deposit on the substrate is extended by the addition of EDTA. The film's crystalline nature, with cubic phases and no impurities, is revealed by the PXRD patterns. The as-deposited films have a uniform coating to the substrates and are pinhole-free and highly uniform (Figure 2(a)). When reacting materials such as EDTA are used as complexing agents, the surface morphology of the deposit's changes accordingly (Figure 2(b)). Every entity has a structure that isn't porous. When the complexing agents were introduced to the parent material, proliferated grains typically appeared in the surface morphology. According to Hall effect measurements, these surfactant-free films are p-type semiconductors that change to n-type upon the addition of complexing agents.

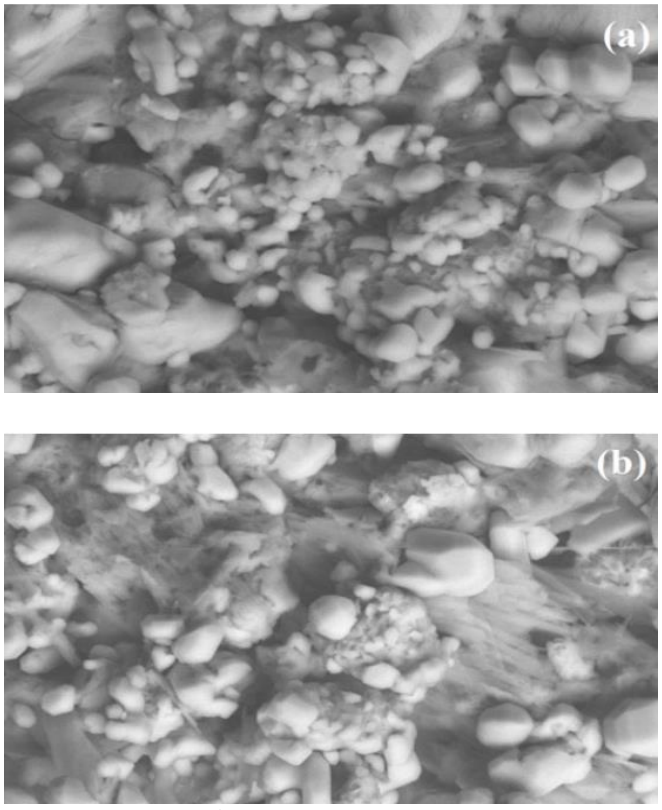


**Fig. 2 SEM images of (a) $CuZnS_2$, and (b) $CuZnS_2$ with EDTA [18]**

Since lead chalcogenide thin films are highly photosensitive in the 0-4 μm spectral range, they are widely used in the infrared methods. The high photosensitivity of PbS film is typically attributed to the activation of halogenide and oxygen spots within the layers. Additionally, the conditions under which the layers are deposited have a significant impact on their microstructure and photoelectric characteristics. Ultrasound and microwave radiation are frequently utilized to create new materials with unique characteristics.

Ultrasound vibrations can lead to the creation of tiny particles with a large surface area. These conditions during ultrasound treatment are effectively used to produce various nanoscale materials, including metals, metal carbides, metal oxides, and metal chalcogenides. Microwave treatment alters the level of order in the solvent and the structure of ionic solvates, changes the electron shell configurations of atoms and molecules, and enhances particle interaction, reduces reaction times, and increases reaction efficiency and rates, while also causing rapid heating of the volume.

The lead precursor (lead acetate) in the solution results in the formation of lead ions. Sodium citrate is employed to make complex lead ions, which prevents the formation of sulfide compounds. The ammonium iodide is used as a selective dopant. A precursor for sulfide ions is thiocarbamide, which is unstable in alkaline solutions. Lead sulfide thin films were grown using chemical bath deposition under thermostatically controlled conditions, with the addition of microwave and ultrasonic irradiation.

The synthesis of thin films took place at 80 °C in Mo-glass beaker reactors, with sital substrates immobilized on specially designed fluoroplastic devices. Deposition time in the microwave oven was standardized at 90 minutes for all PbS thin films. SEM analysis confirmed the nanoscale nature of the thin films, which varied depending on the deposition conditions. The examination of lead sulfide thin films (Figure 3(a)) revealed that they exhibit a fine-crystalline cubic structure [19], with an average crystal size ranging from 90 to 400 nm. During the ultrasonic treatment of the synthesis process (Figure 3(b)), the PbS crystallites lose their pronounced cubic structure and undergo agglomeration.

The average crystallite size decreases to 200 to 350 nm, with significant aggregates present on the film's surface, reaching sizes up to 500 nm. The average size of the submicron particles increased to 150 to 450 nm with the escalation of ultrasonic irradiation power.

However, the visible shape of the particles became more cubic, characteristic of films produced under thermostatic conditions. Given the complex nature of the synthesis process in microwave irradiation, many particles fail to fully form by the end of the deposition process, negatively impacting both the microstructure and the film's thickness and properties.

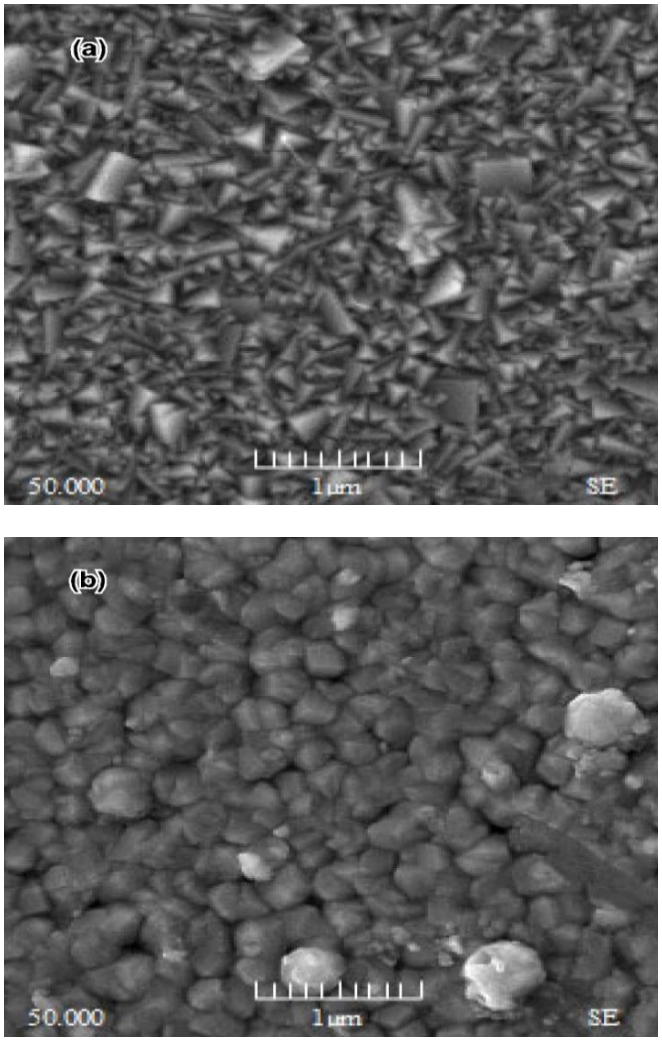


**Fig. 3 SEM images of PbS films deposited at (a) Thermostatically controlled, and (b) Microwave conditions [19]**

$CuFeS_2$ film has a narrow band gap (0.5 eV), higher electrical conductivity value, and Seebeck co-efficient. To optimize the deposition of films, we have a preliminary understanding of the thermal evaporation process of iron (Fe) and copper (Cu) powder. Therefore, thermal evaporation was performed on pristine Fe and Cu, as well as manual mixing of Fe-Cu powders (atomic ratio of 1:1).

Malagutti and co-workers [20] presented a new method to produce films through ball milling, thermal evaporation and sulfidation process. It has been observed that ball milling of metal precursors prior to evaporation is essential for effective mixing of copper and iron elements.

It is noted that a two-phase current (such as 105 A and 140 A) is required during the experiment. Copper and iron explain that using a smaller amount of mass can improve the energy to mass ratio during the evaporation process. They also mentioned that higher vacuum and the proximity between the source and the target improved the adhesion of the films.

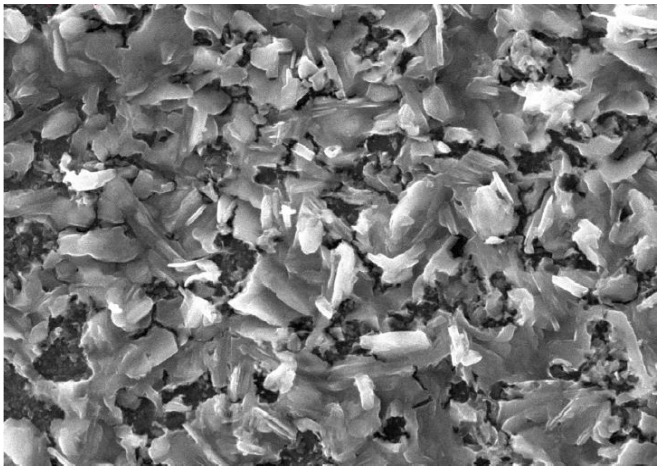

**Fig. 4 SEM image of $CuFeS_2$ films [20]**

As shown in SEM images, the micrometrics grains form bigger (Figure 4) polycrystalline agglomerates with an irregularly shaped microstructure on the surfaces of the films. Chemical maps collected on the same surface suggested that the copper is homogeneously distributed in the samples. While the sulfur and iron are more differentiated on the upper surface of the grains.

There are two different types of ZnS, an II-VI compound semiconductor: cubic and hexagonal. Under standard temperature and pressure settings, it crystallizes as a structure composed of mixed zinc. ZnS has been the subject of intense research recently due to its broad bandgap of 3.6~3.8 eV in the bulk and significant exciton binding energy, which make it a promising material for many optoelectronic devices. ZnS is an important material for UV-LED, flat panel displays, windows for solar cells, and sensors because of its wide bandgap. On tiny glass substrates, zinc sulphate hexahydrate, thiourea, and ammonia (a complexing agent) were used to create ZnS thin films. After 45 minutes, at 60 °C and pH of 9.8, thin and homogeneous films were visible. It has been shown that thiourea hydrolyses more quickly at higher temperatures. This rise leads to a usually low fixation $OH^-$ particle and a relatively high grouping of $S^{2-}$ particles. ZnS precipitation forms in an arrangement when the ionic product of $Zn^{2+}$ and $S^{2-}$ particles exceeds the solubility product of ZnS in the present.

Unexpectedly, the hydrolysis of thiourea is carried out with a low convergence of $OH^-$ particles, which stifles the growth of $Zn(OH)_2$. The decreased population of tiny grains on the substrate's surface is observed in SEM examinations [21], and the as-deposited film has an uneven surface with occasional fissures (Figure 5(a)). The annealed samples (Figure 5(b)) exhibited increasingly uniform and denser surface morphologies devoid of fractures. The medium-sized grains have an arbitrary framing. The opportunity to reorganize the atoms into bigger grain sizes and well-organized primitive crystalline cells is provided by the annealing process.

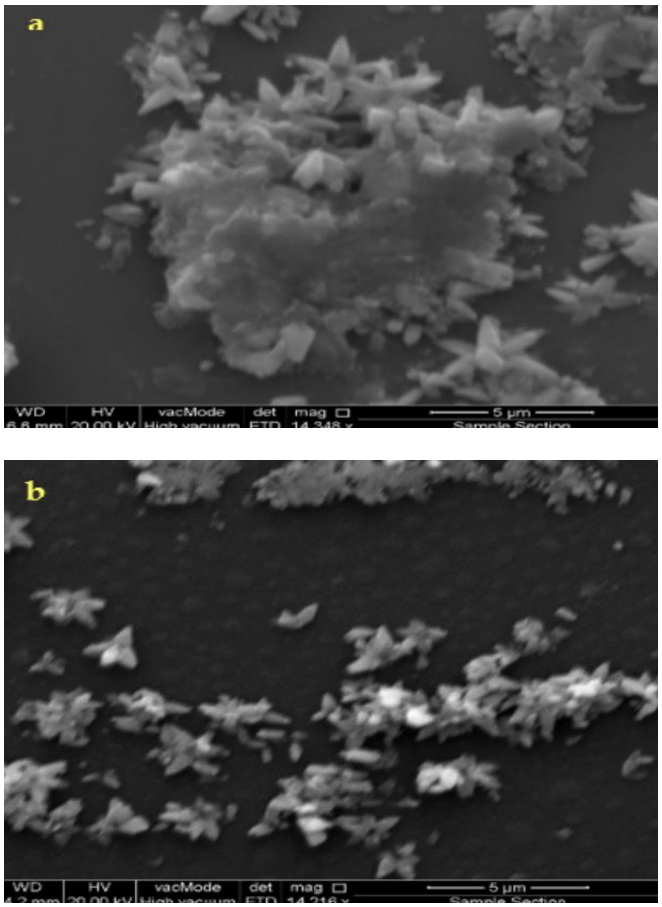


**Fig. 5 SEM images of (a) as-deposited ZnS, and (b) annealed films [21]**

In this study, it is appropriate to use a clustering method for the ZnS film deposition. The implicated ions' clusters accelerate the adsorption process, causing heterogeneous catalysis at the chemical solution/substrate surface. This thickens the film where it functions as a catalytic surface. With a nearly optimum energy bandgap and a wide energy bandgap oxide, tin sulfide (SnS) exhibits amphoteric properties that may lead to grain boundary passivation. In addition to having a relatively high elemental content, SnS can already be produced on a large scale through a variety of sulphidization techniques, which can also be used to convert metals into the corresponding sulphide. Under circumstances (substrate and target distance = 40 mm, vacuum pressure = $10^{-5}$ to $10^{-6}$ Torr, deposition time = less than 5 minutes), tin sulphide has been thermally evaporated onto soda-lime glass substrates. Every thin film that was deposited was pinhole-free [22], consistently thick, and adherent to the substrate. Whereas films thicker than 10 µm showed rougher surface and a darker black color. In addition, experimental results revealed that yellow brown color with smooth surface could be observed for the films deposited with thicknesses less than 4 µm. Obviously, thicker films could be found in lower substrate temperatures, longer deposition times, and higher source temperatures. When the substrate temperature varied from 100 °C to 300 °C while the source temperature remained

constant at 300 °C, samples in EDX studies displayed a trend of decreasing tin concentration. This varied from a mean evaluated composition of sulphur (S 2.2 % and tin (Sn 50.8 %) at 100 °C to sulphur (S 50 %) and tin (Sn 50 %) at 300 °C. The results indicated a trend of rising tin concentration when the source temperature varied between 300 °C and 500 °C while the substrate temperature remained fixed at 300 °C. At 300 °C, the mean evaluated composition was approximately 50.04 atomic % for S and 50 atomic % for S. At 500 °C, the mean composition was approximately 61.3 atomic % and 38.7 atomic %, respectively. During film growth, oxygen was detected and most likely incorporated by diffusion from the soda-lime glass substrate.

The p-type of Cu2ZnSnS4 (CZTS) consists of kesterite and wurtzite in its crystal structure. The kesterite structure has less energy and stability despite its many benefits. The self-doped formation of CZTS results in intrinsic defects like vacancies, antisite defects, and interstitial defects. Its crystal structure is like that of chalcopyrite CIGS. The CuZn antisite defects that result from high-performance CZTS solar cells' Cu-poor and Zn-rich conditions frequently give rise to p-type CZTS semiconductors. Furthermore, the formation of detrimental secondary phases under nonstoichiometric growth conditions necessitates specific CZTS synthesis, as the CZTS phase is a prerequisite for the development of high-efficiency solar cells. A study on the Rapid Thermal Annealing (RTA) of as-electrodeposited CZTS films is presented by Maxim and colleagues [23]. It was observed that a tiny portion of the as-deposited layer crystallized after a brief (5 minutes) annealing period. After 10 minutes, a layer of pinholes with grains ranging in size from 1 to 4 μm forms; after 15 minutes, the grains have grown to be much larger, measuring 4-5 μm. However, morphology analyses were published for samples that were annealed at various rates. The samples that undergo slow annealing have grain sizes of 8–10 μm, while samples that undergo fast annealing have grain sizes of 1-2 μm.

Additionally, SEM observations for samples treated at various temperatures were emphasized. Single independent grains with sizes close to 1-2 μm were present in the CZTS layer at 600 °C. Pinholes are visible and the grain concentration increased to 650 °C. Grain sizes peak at 4-5 μm at 700 °C, but when the temperature rose to 750 °C, the sizes decreased and showed heterogeneous residuals along the grain borders. The RTA is in favor of processing thin absorber films within a thermal budget, and a suitable optimization will raise the ratio of cost to efficiency. Cao and co-workers [24] presented a photo-sintering method that could potentially take the place of the traditional thermal annealing method for CZTS thin-film devices. Because of its adaptable substrate and environmentally friendly process, this technique can be used in a wide range of applications. The broad absorption wavelength range of the photo-sintered CZTS films is 400–1400 nm. A 1.6 eV optical band gap was discovered. There was a noticeable absorbance in the visible spectrum, and in the infrared, a tail that reached longer wavelengths. CZTS exhibits good absorption in the visible range, suggesting that it would be a suitable absorber layer for a photovoltaic device. The as-coated films showed small grains and porous morphology based on SEM images. Due to the higher bank voltage during the photo-sintering process, the CZTS surface generally became rougher and exhibited island-like growth as the grain size and crystallinity increased. The film's particle sizes increased in tandem with an increase in intense pulsed light energy, suggesting that crystallization took place in the CZTS film. Photovoltaic behaviors were studied, power conversion efficiency and short circuit current were found to be 1.01% and 2.96 J/cm$^2$, respectively.

### *3.2. SEM Studies of Metal Selenide Films*

$Cu_2Se$ and its derivatives have drawn a lot of attention lately as potential sources of high dimensionless quality factor thermoelectric materials. Only solid-state techniques can directly convert industrial waste heat into usable electrical energy using thermoelectric materials. They can also be utilized as heat pumps to deliver cooling locally. Despite their many benefits-lightweight, dependable, fully solid-state, and extended service life-thermoelectric materials' low conversion efficiency is the primary reason for their restricted application. Pulsed magnetron sputtering method is used to prepare $Cu_2Se$ thin films (substrate=glass, power supply=500 VA), as described by Yang and colleagues [25]. A magnetic field that is too high will impact the uniformity of the film that is produced and the target material's utilization rate. A magnetic field that is too little will make it difficult to produce glow discharge. The heating and rotating capabilities of the substrate table enhance the film's uniformity and adherence. The outcome of an observation made at a 600-times magnification (Figure 6(a)). The film's surface has a lot of particles on it. Particle size distribution was nearly consistent, with an approximate range of 3–5 μm. The surface of the film at 20,000 magnifications (Figure 6(b)). Smaller particles were seen at this point on the film's surface. However, scientists have pointed out that the produced films have a thickness of roughly 100 nm and are somewhat rough. There were a lot of haphazard grey particles that were somewhat smaller than hexagonal particles.

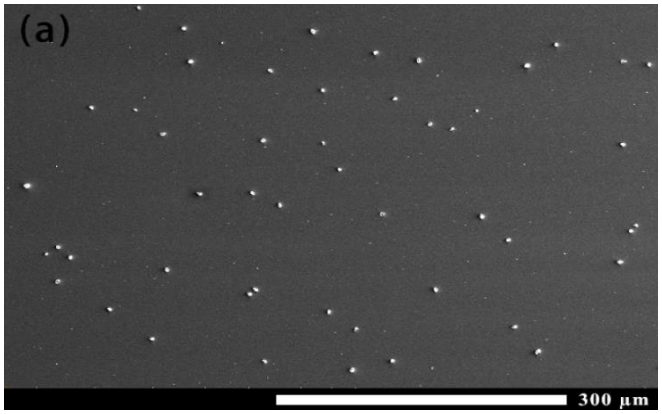

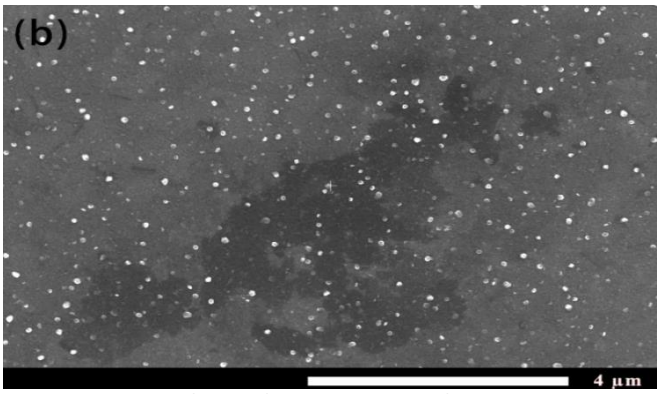


**Fig. 6 SEM images of $Cu_2Se$ films. (a) 600 magnifications, and (b) 20,000 magnifications [25]**

The SEM images in Figure 7 depict [26] the top view of $CuInSe_2$ thin films grown on Mo/soda lime glass. Prior to applying the back contact layer, the soda lime glass substrates underwent cleaning with acetic acid and deionized water to eliminate organic contamination. The CISe films with Cu/In ratios ranging from 0.87 to 0.95 manifest a distinct polyhedral-shaped morphology on their surfaces, indicating a chalcopyrite phase. As the Cu content increases, the grain sizes of the CISe films also increase. Specifically, for Cu/In ratios of 0.87 and 0.95, the grain sizes were estimated to be approximately 0.59 and 1.26 µm, respectively. In the Cu-rich state with Cu/In ratios of 1.27 and 1.11, the grains displayed particle-like shapes with sizes measuring 0.91 and 1.14 micrometers, respectively. Many Cu-Se compounds exhibit particle-like shapes.

Researchers have successfully demonstrated low bandgap CISe thin-film photodetectors that operate in the Near-InfraRed (NIR) range. The bandgap value has been adjusted by varying the Cu/In ratio from 1.02 to 0.87. Zinc selenide (ZnSe) has unique physical properties, including high electrical conductivity, excellent photosensitivity, and environmental friendliness. In addition to environmental factors, ZnSe's wider band gap energy (about 2.67 eV) than CdS is raising the prospect of bettering photocurrent and blue light radiation transmission.

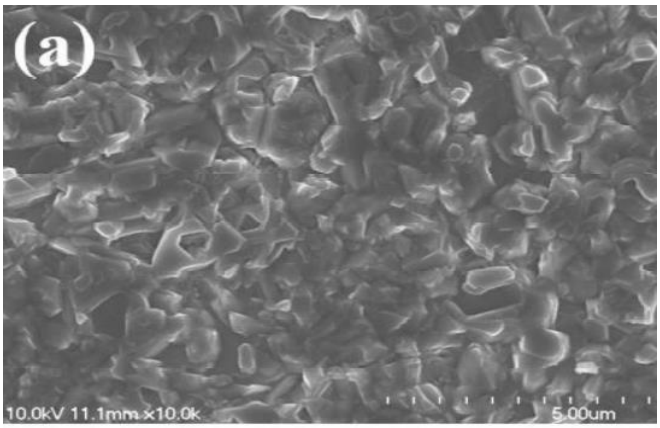


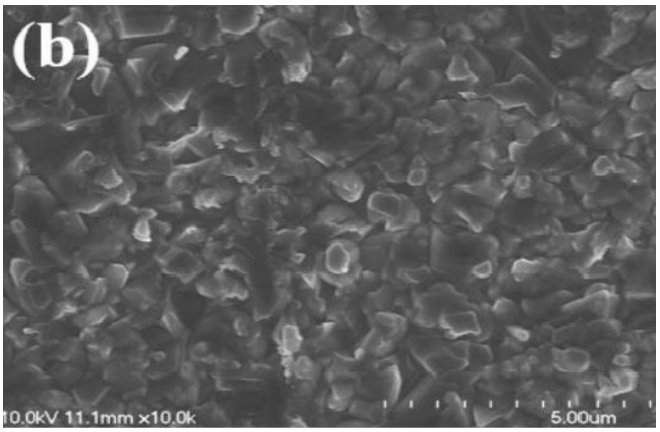


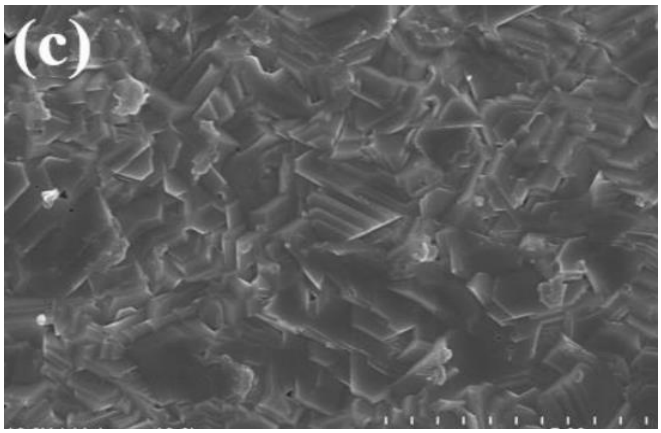


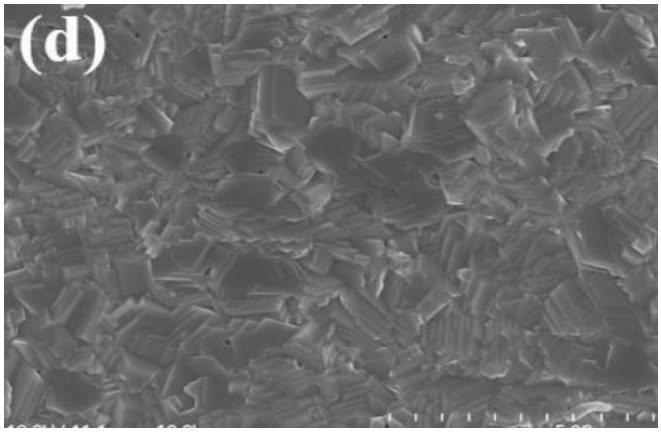


**Fig. 7 SEM images of CISe films with Cu/In ratios of (a) 1.27, (b) 1.11, (c) 0.95, and (d) 0.87 [26]**

Interestingly, ZnSe material could be used as buffer material in various solar cell configurations according to many reports. Optical glass substrates were subjected to binary ZnSe thin film deposition using RF magnetron sputtering (target-to-substrate distance = 8 cm, substrate temperature = 220 °C, sputtering time = 30 min, RF power = 60 W, gas pressure=0.86 Pa). It was observed that as the RF power is increased, the sample's crystalline quality increases. Because more RF power increases electron mobility, the ionization efficiency of argon gas atoms is further enhanced. Thus, the

highly energized inert argon ions give the sputtering adatoms on the growing surface translational kinetic energy, improving their surface diffusion and ultimately producing films with superior crystalline structure. The ZnSe films obtained in SEM investigations [27] are compact and sputtered on glass substrates with good conformality (Figure 8).

It is evident that as RF power increases, film thickness rises from 37 nm (60 W), 170 nm (80 W), 271 nm (100 W), and 351 nm (120 W). As the rate of deposition decreases to 120 W.

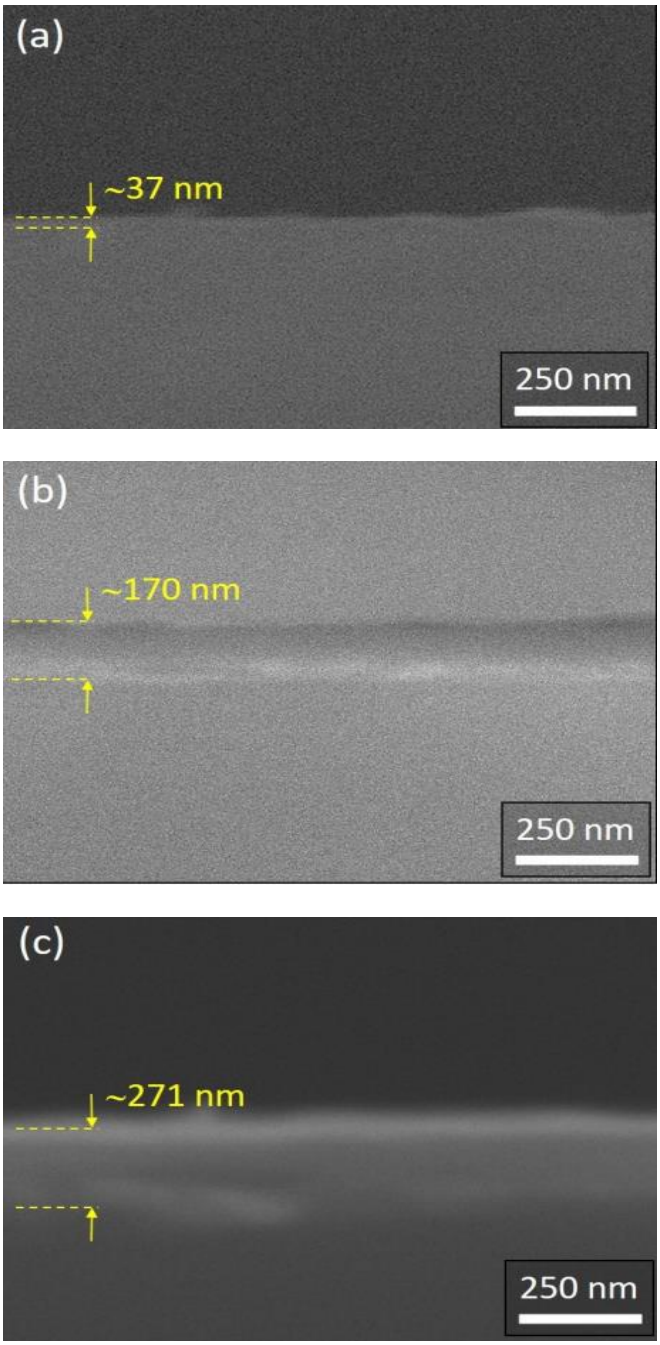


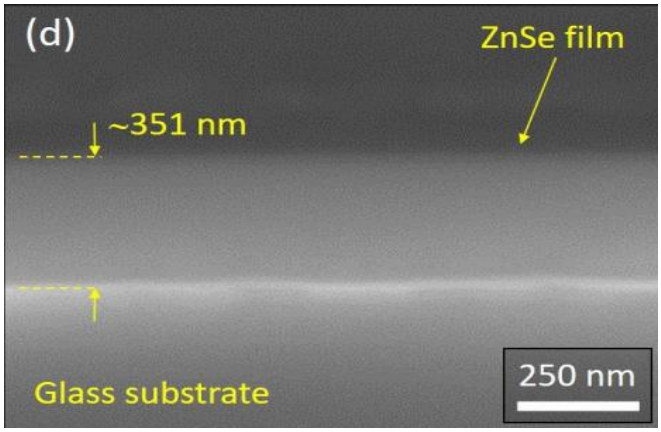


**Fig. 8 SEM images of ZnSe films prepared under different RF power values (a) 60 W, (b) 80 W, (c) 100 W, and (d) 120 W [27]**

This is because there is a higher deposition rate because of the particles' increased kinetic energy and velocity as they splatter away from the target. However, the slowdown of the observed increase in deposition rate towards 120 W can be attributed to the injection of ions into the target with an excessively high energy, which results in an energy and quantity loss of argon ions and further reduces the deposition rate.

CdSe is a significant material in the advancement of numerous contemporary solid-state device technologies, including solar cells, high-efficiency thin films, transistors, light-emitting diodes, electron beam pumped lasers, electroluminescent devices, and gamma-ray detectors. Recently, considerable focus has been directed towards exploring the electrical and optical characteristics of CdSe thin films to enhance device performance. A crystalline cadmium selenide film has been successfully deposited onto glass substrates using cadmium sulfate, triethanolamine, sodium hydroxide, ammonia solution, and sodium selenosulfate under controlled conditions (pH = 11.5, temperature = 50 ℃, rotation speed = 70 rpm, duration = 2 hours). The resulting films exhibited uniformity, strong adhesion to the glass substrate, and a specularly reflective surface.

Furthermore, these films displayed smooth surfaces (Figure 9) characterized by spherical grains of nearly uniform size. Most of the grains were interconnected, and no pores were observed [28]. Compositional analysis conducted via EDX revealed a composition of 53.87% cadmium and 46.13% selenium, indicating an excess of cadmium. The crystalline structure of the deposited sample was identified as hexagonal wurtzite, with a band gap energy of 2.18 eV. The electrical resistivity of the CdSe thin film was measured at $10^{-6}$ $(\Omega\ cm)^{-1}$. On non-conducting glass substrates, nickel selenide thin films have been deposited using the chemical bath method. The tartarate bath contains sodium selenium sulfate, hydrazine hydrate, and nickel sulphate octahydrate. The grown hexagonal phase films had a black color, were uniform, and were well adherent.

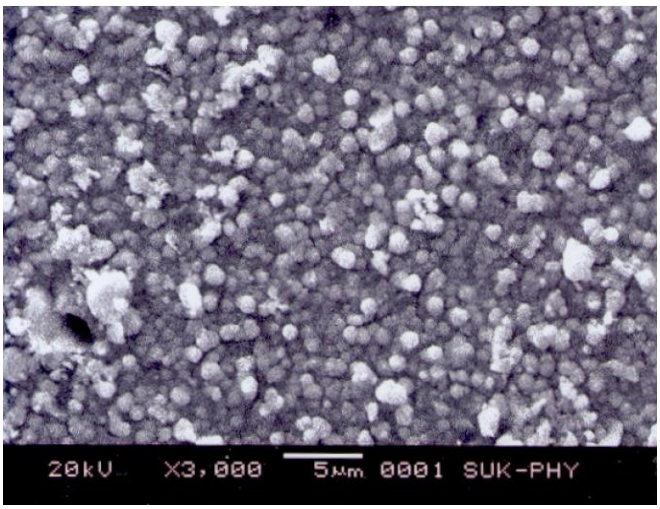


**Fig. 9 SEM image of CdSe films [28]**

Throughout the film growth process, the $Ni^{2+}$ concentrations are regulated by the complexation of $Ni^{2+}$ ions with tartaric acid in the reaction bath, produced water-soluble Ni–tartarate complex. In an alkaline medium, the Ni-tartarate complex and sodium selenosulphate complex dissociate. NiSe thin film formation is favored by slow increase in temperature which results in an increase in kinetic energy. The gradual release of $Ni^{2+}$ and $Se^{2-}$ ions from the solution is the basis for the deposition process. On the glass substrate, an ion-by-ion growth mechanism facilitates the formation of the film. The nickel selenide thin film is uniform, well-covered [29], and free of pinholes and cracks on the glass substrate, according to the SEM images (at a magnification of 10,000). The 400 nm grains have a spherical shape and are clearly defined.

Doped ZnSe nanostructures have been documented in several works. Microwave assisted solvothermal synthesis of Cu doped ZnSe quantum dots reveal that mercaptoacetic acid, the capping agent, works well for creating nanoprobes for bioimaging applications. It has been discovered that the concentration quenching effects of Europium doped ZnSe lead to good color tunability, ranging from blue to yellow ocher in colloidal quantum dots. On the surface of ZnSe quantum dots, lower europium doping resulted in the formation of $Eu_2O_3$ & EuO, whereas higher concentrations produced more oxygen-rich $Eu_3O_4$ on the samples' surface. It has been demonstrated that the formation of highly porous nanocomposites was induced by ZnSe nanoparticles embedded in porous Nd doped carbon nanocubes. Good electrochemical behaviours will be indicated in these samples, and well-developed porosity structure resulted in easy lithium ions diffusion, which could be observed in lithium-ion batteries. Using sodium selenite as a precursor and a temperature of 180 °C, nickel doped zinc selenide nanoparticles were created hydrothermally. The samples' effective crystallite sizes were well below 15 nm, indicating improved nano crystallinity. SEM images demonstrate how the Ostwald ripening mechanism produced spherical particles at the micron scale [30]. However, in photoluminescence spectroscopy studies, the concentration of the dopant (nickel) determines the strength of emission intensity. Researchers have determined that there is an increase in emission intensity with dopant concentration.

Because SnSe has the highest known thermoelectric figure of merit, thermoelectric generators may be able to use it. SnSe is a good option for sustainable photonic and electronic systems since it also contains elements that are both plentiful and safe on Earth. The polymer's surface begins to form SnSe films, which create novel composite materials with unique combinations of chemical and physical properties. These materials present exciting new possibilities for current and future devices. When it comes to the use of films, these composites frequently help to significantly reduce costs by utilizing inexpensive substrates while maintaining the coating material's properties. As a result, a lot of research has concentrated on methods for creating superior SnSe films. According to Zainal and colleagues [31], p-type SnSe film was electrochemically deposited on a tin substrate utilizing three standard electrode cells in an aqueous solution containing $SnCl_2$ and $Na_2SeO_3$. The results of the experiment verified that SnSe films are produced in a bath with an equal electrolyte ratio or a higher concentration of $Na_2SeO_3$. SEM micrographs of films made with varying $Na_2SeO_3$ concentrations and a fixed 0.01 M $SnCl_2$ concentration. The deposits are crystalline and the concentration of $Na_2SeO_3$ affects the grain size. Higher photoactivity and smaller crystal sizes are caused by higher $Na_2SeO_3$. Because of the crystal's compactness when illuminated, photoactivity of films and its crystal grain size are therefore correlated. This leads to a higher rate of electron-hole pair generation per unit area, which in turn promotes higher photocurrent.

Tin selenide films were synthesized in the orthorhombic phase on polyamide sheets using a two-stage adsorption/diffusion process. The polyamide sheets have changed color from transparent, light yellow and finally to slightly reddish in a span of sixty to ninety minutes. It signifies the breakdown of dispersed $SeS_2O_6^{2-}$ ions within the polymer. The prepared films displayed varying sizes of crystallinity based on their formation condition, as observed by the SEM images [32]. Following the initial phase of selenium formation, the distinctive domains of the polyamide structure become visible. Moreover, when crystallites and their agglomerates in the 10-400 nm range are dispersed randomly across the polymer surface, the film lacks a distinct morphology. According to the results of the EDX analysis, the sample's established average atomic percentages for selenium, sulfur, and oxygen are 28.76 at%, 3.12 at%, and 68.12 at%, respectively. This suggests that most selenotrithionate anions break down into intermediates during the adsorption/diffusion process. Consequently, elemental selenium is most likely the composition of the crystallites that are visible on the polymer surface. Following the second phase of the procedure, the surface's appearance underwent a cardinal change. On the

polymer surface, well-visible films are produced, and the conditions surrounding their formation process determine how they look. The iron selenide system exhibits a range of structures in addition to two homogeneous and stable phases, a-FeSe and $FeSe_2$. The crystal structure of the a-FeSe phase is tetragonal and hexagonal. $FeSe_2$ crystallizes as a cubic structure and as an orthorhombic marcasite type. Using ethylenediaminetetraacetic acid (a complexing agent) and a chemical bath containing $Fe(NO_3)_3$ solution and $Na_2SeSO_3$ solution, iron selenide films were created at room temperature on glass substrates. The resulting films had a uniform orange-brown color, were strongly bonded to the substrate, and had a specular reflection. According to Ubale's [33] SEM investigation, the FeSe film that is deposited on the substrate is uniformly porous and has irregularly shaped grains covering it. Two to three mm long nano rectangular rods and plates are seen at various locations on the substrate surface.

Numerous locations also show incompletely formed nanorods and nanoplates. Only the elements iron (Fe) and selenium (Se) are subjected to elemental analysis. The atomic percentage of Fe:Se on average was 53:47, indicating a high iron content in the deposited film. Conversely, p-type $FeSe_2$ films have been thought to be the perfect material to use in the creation of solar energy systems. Their band-gap energy is approximately 1 eV, and they exhibit a high optical absorption coefficient ($5X10^5$ $cm^{-1}$ for $\lambda$ less than 800 nm). Using oleylamine as a reducing agent and iron (III) acetylacetonate and element selenium as raw materials, Qin and colleagues [34] created $FeSe_2$ particles by a hot-injection technique. This one-step synthesis approach results in limited growth control of the $FeSe_2$ particles, despite being a straightforward, non-toxic, and inexpensive method for creating $FeSe_2$ particles. This is because the growth process of $FeSe_2$ particles and the reduction process of Se occur simultaneously. $FeSe_2$ particles that resemble flowers and have micron-sized particles are clearly visible in the SEM analysis. These products are made up of $FeSe_2$ nanorods that have edged that range in length from 50 to 80 nm.

The as-prepared $FeSe_2$ particles contain the elements Fe and Se, as shown by the EDX spectra. The molar ratio of Se/Fe is 1.998, which is extremely close to the stoichiometric ratio of $FeSe_2$. $Cu(In,Ga)Se_2$ (CIGS) films are made via co-evaporation or a two-step process (sulfurization following selenium). Thin-film CIGS solar cells, whose CIGS films were made via the co-evaporation process, have achieved efficiencies of more than 20 %. It is simple to scale up the two-step CIGS film preparation procedure for mass production. $H_2Se$ gas is usually used in a two-step process to selenium the metal precursors to achieve high performance. $H_2Se$ gas, however, is flammable and extremely toxic. Extreme caution must be exercised when processing $H_2Se$. According to SEM studies [35], the number of voids in CIGS films selenium-treated at a high selenium flow rate was significantly reduced for metal precursors with either low or high Ga contents. The CIGS films that were selenium-extracted at a high flow rate produced well-faceted grains, which is advantageous for the CIGS films' surface morphology. The shunt path could be reduced because of compact and dense morphologies. As a result, open-circuit voltage and fill factor were improved.

### *3.3. SEM Studies of Metal Telluride Films*

When used as a photocathode material for Photoelectrochemical (PEC) water splitting and absorbing materials in photovoltaic cells, cadmium telluride (CdTe) offers several appealing characteristics. It possesses a high light absorption coefficient-$10^4$ $cm^{-1}$ in the visible light range-and a direct band gap of 1.45 eV. For the high material utilization and simple operation of producing CdTe films in large quantities, electrochemical deposition is the perfect technique. The method of electrodeposition has various benefits. It can easily function, for instance, in an environment with low vacuum or high temperature. Both p-type and n-type CdTe have been found to deposit readily, with electrodeposition potential being identified as the critical element. Tellurium-rich CdTe films have been synthesized by Ling and colleagues [36] utilizing a three-electrode arrangement. The working, reference, and counter electrodes in this setup were FTO glass, Ag/AgCl in a saturated aqueous KCl solution, and a Pt wire, in that order. According to SEM pictures (Figure 10), the thickness of CdTe thin films increases from 1.08 µm to 2.7 µm with increasing deposition time (1 hour to 2.5 hours). It was noticed that certain restricted particles with distinct sizes are also generated, and some islanding was formed. The thin films that were formed between 1.5 and 2 hours showed good PEC performance, the greatest photocurrent, good morphology, and outstanding optical characteristics.

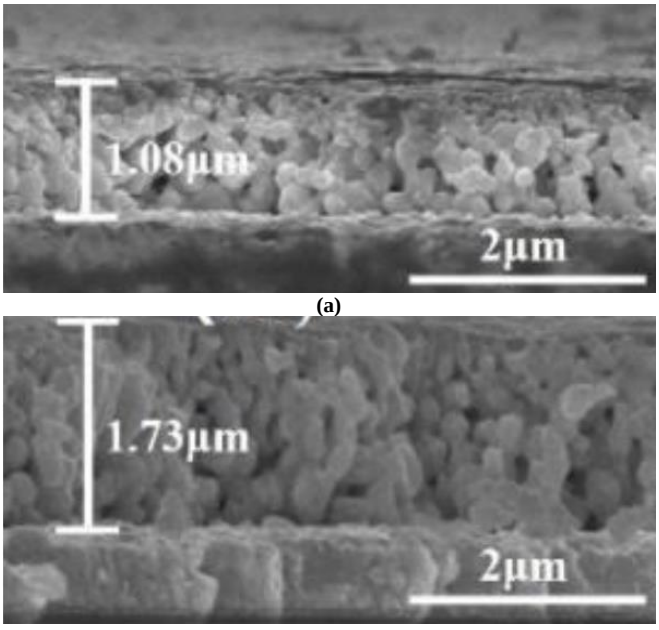


**Fig. 10 SEM images of CdTe films (a) 1 hour, and (b) 1.5 hours [36]**

Cadmium telluride films have been effectively synthesized using an electrodeposition method from an aqueous electrolyte solution comprising cadmium chloride and tellurium dioxide. The optimal cathodic potential identified is 698 mV relative to the standard calomel electrode within a three-electrode configuration. X-ray diffraction analysis reveals a polycrystalline structure in the as-deposited CdTe thin films, with peak intensities increasing following treatment with $CdCl_2$. The electrical resistivity of the as-deposited films is approximately $10^4$ Ω·cm.

Scanning electron microscopy (Figure 11) indicates that the samples treated with $CdCl_2$ exhibit greater roughness and larger grain sizes compared to those grown using a $CdSO_4$ precursor. The as-deposited CdTe demonstrates grain sizes ranging from 150 to 200 nm [37]. As the annealing temperature rises, the grains begin to merge, resulting in larger grain formations. The $CdCl_2$-treated CdTe at temperatures of 420 and 450 °C displays grain sizes in the ranges of 700-900 nm and 1000-4000 nm, respectively.

The inclusion of $CdCl_2$ during thermal treatment facilitates the merging of smaller crystallites into larger crystals, thereby enhancing the quality of the material layers. However, heat treatment at temperatures of 500 °C and above appears to create gaps between grains, leading to a deterioration of the layers. In the case of the sample annealed at 550 °C, the FTO surface becomes visible, as the CdTe layer fails to withstand the high temperature, resulting in material loss.

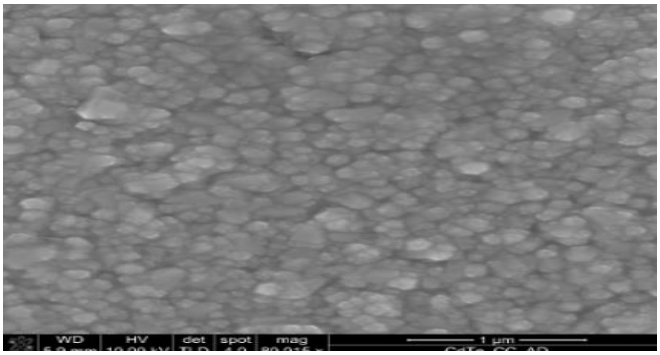

**(a)**

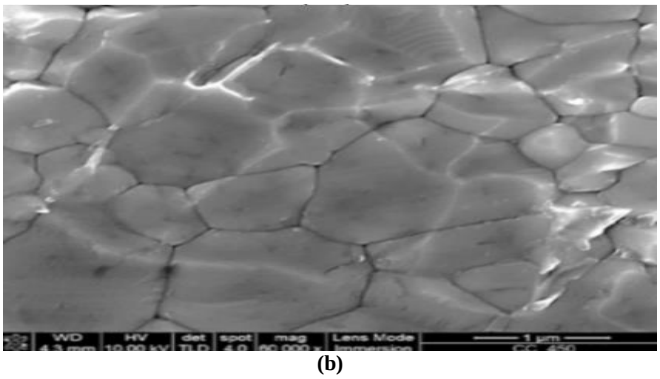

**(b)**

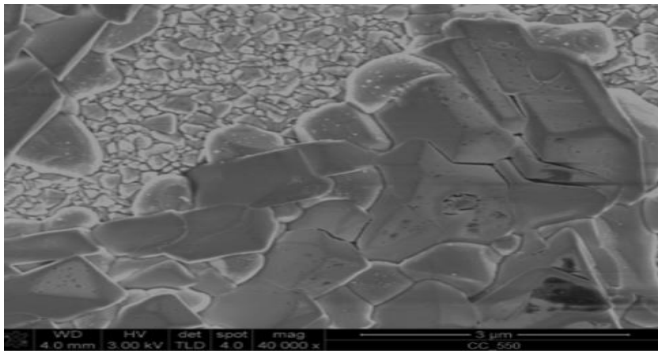

**(c)**

**Fig. 11 SEM images of CdTe films (a) As-deposited, (b) Annealed at 450°C, and (c) Annealed at 550°C**

Zinc tellurium thin film has a direct band gap that ranges from 1.7eV to 2.6eV. The energy gap of semiconductor zinc telluride (ZnTe) depends on various factors such as the preparation method, temperature for synthesis, and other compounds used as sources for the elements of zinc and tellurium and this material possesses high optical absorption coefficient. It is therefore used in optoelectronics and microelectronics devices like X-ray imaging systems, thin film transistors, and detectors. Zinc sulphate and sodium teleurosulphate were used in the chemical bath deposition synthesis of ZnTe thin films [pH=10.5, temperature=369 K, deposition time=470 min]. Triethanolamine has acted as a ligand to complex the $Zn^{2+}$ ions during the formation of a water-soluble complex with it called Zn-TEA so that its concentration would be controlled. In alkaline solution, sodium telenosulfate dissociates while Zn-TEA complex also decomposes into its constituents. As when precipitating at lower temperatures due to reduced kinetic energy is possible, making it metastable form. Thermal decomposition gives out metal ions using metastable complex whereas in an alkaline medium hydrolysis of sodium telenosulphate leads to $Te^{2-}$ ions being formed in an aqueous solution. SEM images (Figure 12) of 'as deposited' thin films showed uniform grain size nanoparticles attached to substrate material that had been grown over its surface. Annealed samples showed a distribution of spherical grains almost having similar size [38].

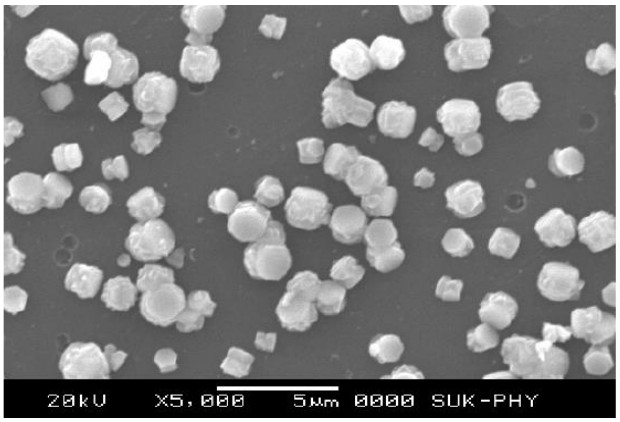


**(a)**

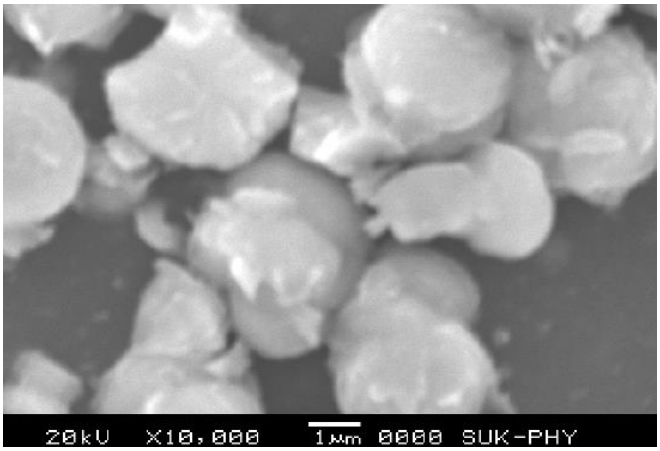


**(b)**

**Fig. 12 SEM images of (a) as-deposited ZnTe films, and (b) Annealed ZnTe films [38]**

Tantalum (Ta) is an element in chemistry with the atomic number 73 and symbol Ta. Tantalum is a blue-gray transition metal that is extremely resistant to corrosion and ductile, hard, and lustrous. To enhance the chalcogenide film's performance, the Ta element was selected as the dopant. These samples were made using a magnetron co-sputtering technique on fused quartz and Si substrates, and they were annealed for 30 minutes at 450 °C. As the concentration of Ta doping increases, the film thickness increases while the crystallinity decreases. Ta doping concentration can be used to modify the performance of InTe films. These films could be used in optical limiters due to high transmittance properties. According to Chunmin's SEM images [39], the estimated film thickness ranged from 306 nm to 356 nm. Main Ta-doped InTe layer, and silicon substrate can be easily identified. SEM analysi confirmed that marginal remnants were left over after cutting the sample. It was reported what the Ta-doped InTe thin films from EDX were made of.

It is evident that when the sputtering power was increased, so did the thickness and weight percentage of the Ta dopant. $CuInTe_2$, a ternary chalcopyrite compound, has been the subject of much research recently due to its possible use in multijunction thin-film solar cells. Using flash evaporation at various substrate temperatures, $CuInTe_2$ thin films have been deposited [40]. Amorphous films were deposited on substrates that were accidentally heated. These films demonstrated the presence of the binary compounds on the film surface and the presence of the chalcopyrite structure's distinctive peaks at substrate temperatures higher than 100 °C. Using spray pyrolysis, thin films were grown at 350 °C on glass substrates. The starting materials were tellurium tetrachloride, indium tri-chloride, and chloride. The solution was sprayed at a pressure of 12 kg/cm$^2$. The resulting film has a grain size of 268 nm and a dense, homogeneous, porous growth morphology. The grains of nanoscale are evenly spaced across the surface. The grains are uniformly sized and shaped, though small. At low temperatures, grain boundary effects are more prominent. The variable Hopping conduction mechanism seems to be active at very low temperatures [41]. Using a brush, the electrodeposition technique has been used to deposit films with a thickness of 200–400 nm on transparent glass substrates at temperatures ranging from 30° to 80°C [42]. According to a report, the small crystalline size causes the band gap to gradually increase as the substrate temperature decreases. Using an electrodeposition method with $CuSO_4$, $In_2(SO_4)_3$, and $TeO_2$ solution, thin films were deposited on indium doped tin oxide coated glass substrates. Reports were made regarding the surface morphology of films electrodeposited at 65 ºC with a deposition potential of -900 mV versus SCE. It is noted that the surface is uniformly smooth and covered in grains with a spherical shape. The grains are evenly spaced across the film's whole surface [43]. The grains, which are aggregates of numerous tiny crystallites, are visible. A larger grain is created by the grouping of several smaller crystallites together. It was discovered that the grain sizes fall within the range of 0.14 and 0.62 μm. It is discovered that the grains have an average size of 0.36 μm.

### *3.4. SEM Studies of Metal Oxide Films*

ZnO nanorods were synthesized and dispersed within a polyvinyl butyral matrix using the sol–gel method, producing homogenous nanocomposite films [44]. The main sources of zinc ions and the precursor solution were zinc salts, such as zinc acetate or zinc nitrate. Zinc hydroxide was more easily precipitated under controlled conditions when a hydroxide source (sodium hydroxide or ammonium hydroxide) was added. The precipitate was then thermally broken down to produce the desired ZnO particles. The procedure was carried out at a regulated temperature to guarantee the creation of crystalline ZnO with distinct morphological characteristics. The purity, size, and structure of the ZnO particles were largely determined by the reagent selection and reaction parameters. The ZnO rod-like structures with uniform morphology (Figure 13) and well-defined dimensions are visible in the micrographs (figure). Additionally, elemental analysis showed that the ZnO particles were uniformly and homogeneously elemental.

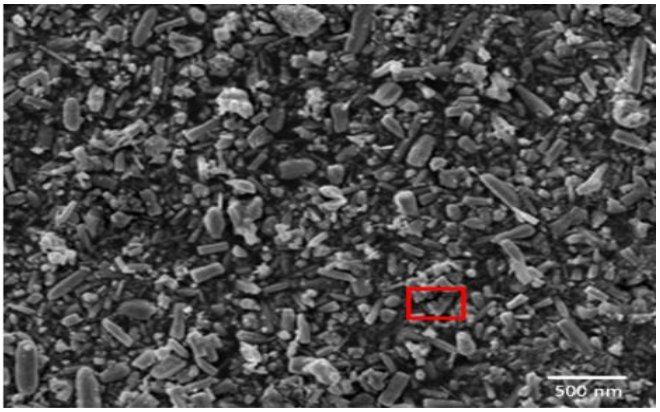


**Fig. 13 SEM image of ZnO films [44]**

Cupric oxide, a type of p-type semiconductor oxide, is a highly adaptable material known for its narrow band gap of 1.4 electron volts, attributed to an excess of oxygen and its exceptional ability to withstand high temperatures. It forms a monoclinic crystal structure with specific dimensions: a = 4.684 Å, b = 3.425 Å, c = 5.129 Å, and b = 99.28º, where CuO units are linked together, and copper atoms bond with oxygen in a plane. Cupric oxide stands out among the monoxides of the 3d transition elements for its square planar arrangement of copper atoms with oxygen in its monoclinic structure. In its pure state, cupric oxide behaves almost like an electrical insulator. However, during the manufacturing process, various defects such as structural flaws, point defects, and impurities from reactants or the substrate materials can introduce deviations from the ideal stoichiometry. Cupric oxide films have been successfully created using the chemical bath deposition method, which involves the use of copper (II) nitrate ($Cu(NO_3)_2$) and ammonia. Substrates made of commercial microscope glass slides were utilized as the base. Prior to the deposition, the substrates underwent cleaning through ultrasonic treatment in a solution of toluene, acetone, and ethanol, followed by a rinse with distilled water. The concentration of ammonia is crucial for controlling the thin film deposition process, as it acts as a chelating agent and adjusts the pH of the deposition solution.

Figure 14 displays top-view SEM images of the resulting film, showing uniform and dense films in the form of elliptic sheets. These sheets are of consistent shape and thickness, with dimensions approximately 600 nm by 100 nm. The sheets stack closely together, leading to a specific orientation. Comparing SEM images of two samples [45], it's evident that changes in the ammonia volume in the deposition system have minimal impact on the film's micro-morphology. The film obtained with an ammonia volume of 2.7 mL exhibits a slightly random arrangement of sheets, and the grain size of these sheets is notably smaller. For preparing nickel oxide thin films [46], spray pyrolysis deposition is used (solution volume: 60 mL, substrate temperature: 350 °C, carrier gas: compressed air, spray rate: 6 mL/min, motor rotation speed: 0.6 cycles per second).

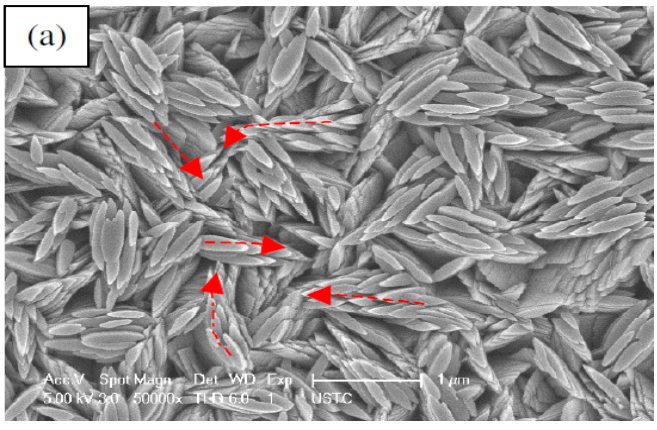


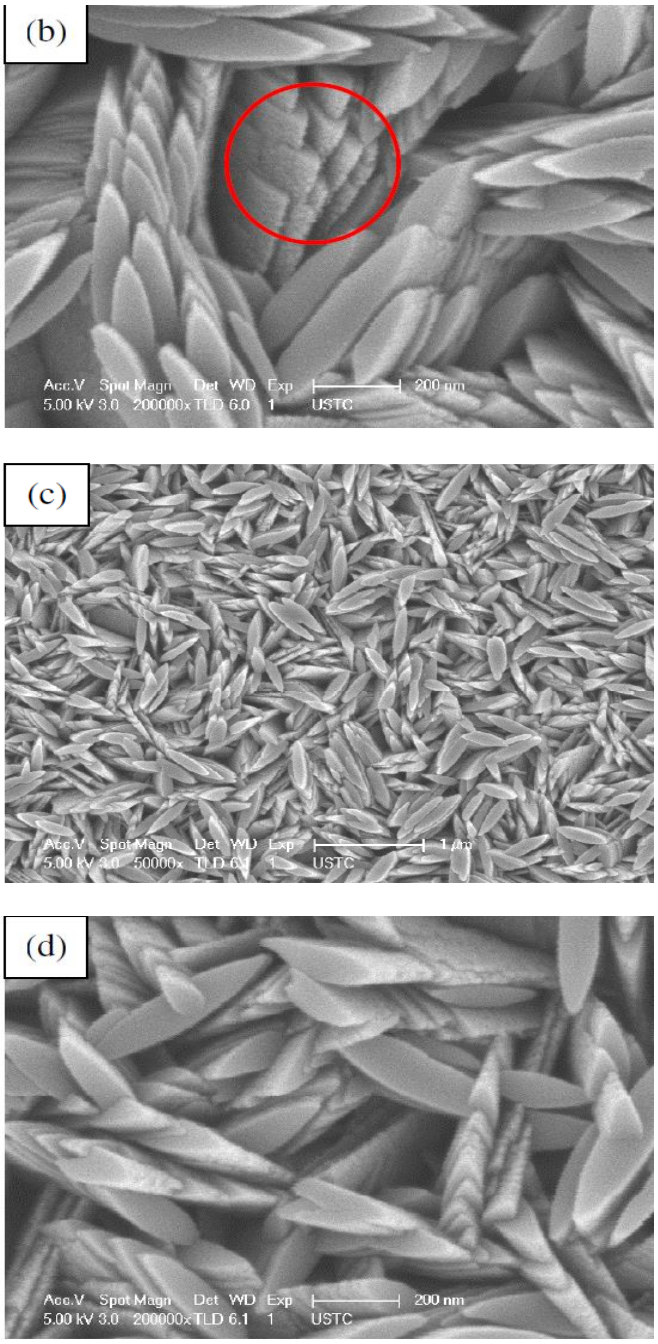


**Fig. 14 SEM images of prepared films using ammonia (a), (b) 3 mL, and (c), (d) 2.7 mL [45]**

This technique is one of the most appealing ways to prepare films because it uses a basic apparatus to create the film in the air during spray pyrolysis deposition. The process known as "pyrosol technique," in which a source solution is sprayed on the heated substrate to be deposited as a film, is essentially the same as spray pyrolysis deposition. To put it another way, during the atomization process, tiny droplets of the source solution splash, evaporate, and leave behind a dry precipitate that undergoes thermal breakdown. According to SEM studies, annealing under vacuum will result in the

development of more porosity and rougher morphology. Samples showed a cubic phase, and annealed films had a higher level of crystallinity. Cobalt oxide, a type of transition metal oxide, shows great potential in various areas including smart optical windows, display technologies, glass and ceramic pigments, and gas sensors. Among the different cobalt oxide oxidation states, $Co_3O_4$ is the most stable, possessing favorable electrochemical properties and a spinel crystal structure for applications in energy storage.

The effectiveness of $Co_3O_4$ is influenced by its microstructure, including grain size, porosity, and crystallinity. Films of nickel-doped $Co_3O_4$ were created on Fluorine doped Tin Oxide (FTO) surfaces by varying the nickel content [47] through a spray pyrolyzed method at 300 ºC. The addition of nickel to $Co_3O_4$ did not change its crystal structure and resulted in films with the highest purity. The addition of nickel at different levels led to a minimal shift in the diffraction peak. Scanning electron microscopy images (Figure 15) of the nickel-doped $Co_3O_4$ films revealed the formation of microspheres [Jasmin, 2023], with the surface becoming more porous at a nickel concentration of 0.05M.

This led to the development of a sample with the most uniform size and structure, which enhanced the surface area of cobalt oxide. SEM analysis showed that the films had sufficient porosity, essential for their use in electrochemical applications. Elemental analysis confirmed the presence of cobalt, nickel, and oxygen in the films. As anticipated, the cobalt oxide doping concentration increased with the nickel content. Using the spray pyrolysis method [48], antimony doped tin oxide ($SnSbO_2$) thin films were deposited onto optical glass slides (nozzle to substrate distance: 40 cm, substrate temperature: 793 K, spray angle: 45º, precursors: antimony trichloride, stannous chloride).

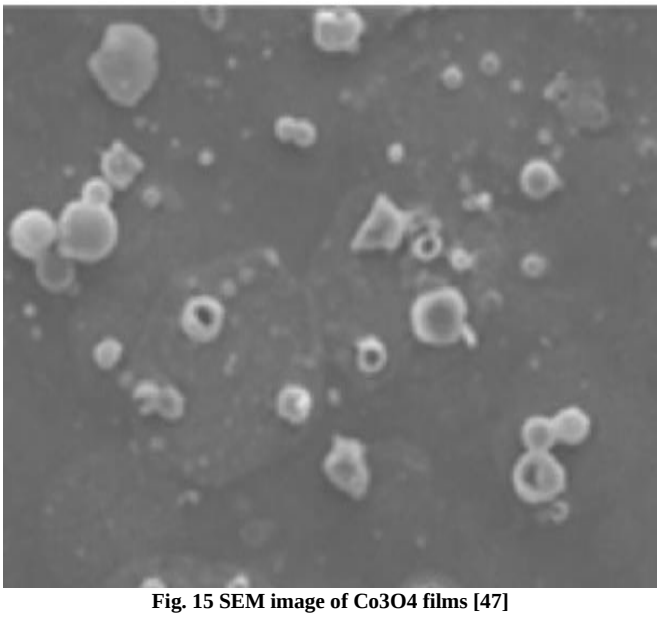

**Fig. 15 SEM image of Co3O4 films [47]**

Triangular-shaped, uniformly sized grains define the undoped film ($SnO_2$). The smaller grains became visible at the surface. As Sb doping increased, so did the quantity of smaller grains (Figure 16). On the surface of antimony-doped films (4% weight) for those with a preferred orientation along the (200) plane, needle-shaped grains have formed. The needle-shaped grains were not present in the film doped with 2% weight Sb. This suggests that the dopant concentration affects the film's grain size.

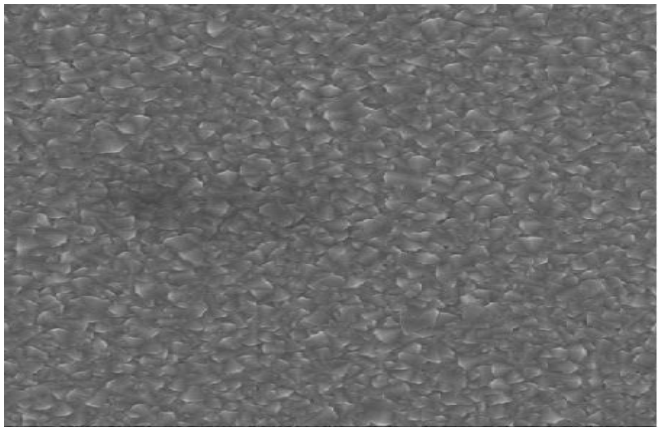

**(a)**

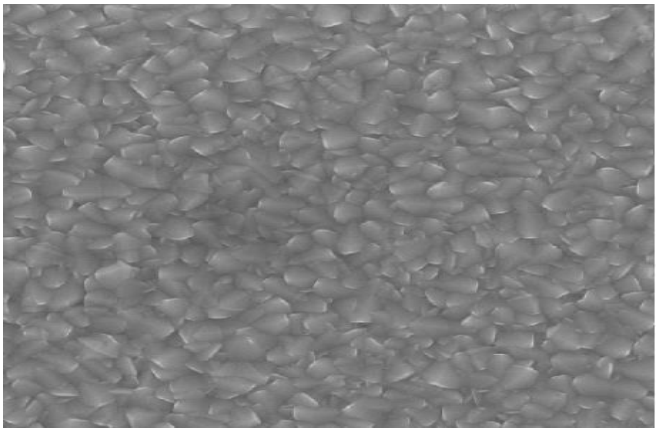

**(b)**

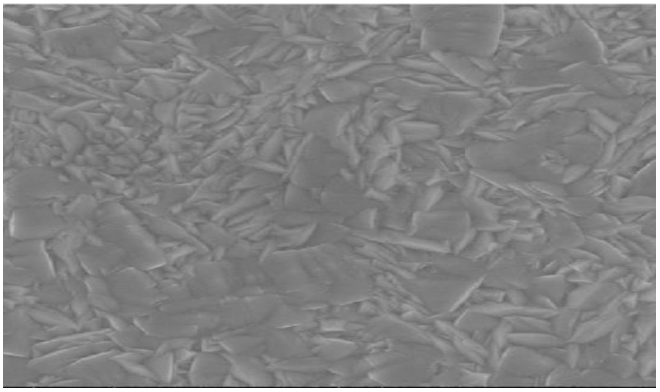

**(c)**

**Fig. 16 SEM images of $SnO_2$:Sb films obtained for different deposition concentrations (a) 0 wt. %, (b) 2 wt. %, and (c) 4 wt. % [48]**

Zinc oxide, zinc magnesium oxide (ZnMgO), and zinc manganese oxide (ZnMnO) thin films have been prepared on a glass substrate [49] by sequential ionic layer adsorption and reaction. The surface formation of nanorods was observed in the pure ZnO thin films. There were no cracks and the ZnMnO film showed spindle-shaped grains (Figure 17(b)). It demonstrates the formation of uniformly distributed sub-micrometer crystallites across the surface.

There appears to be some agglomeration of tiny crystallites in specific areas of the film surface. The ZnMgO films showed a uniform covering of the entire surface with good adherence, as well as a smooth and spindle-like structure (figure 17(c)). The effective doping of 'Mn' and 'Mg' into ZnO thin films is confirmed by EDX characterization. Additionally, the adherence of carbon tape on the study used for the analysis is the source of elemental carbon.

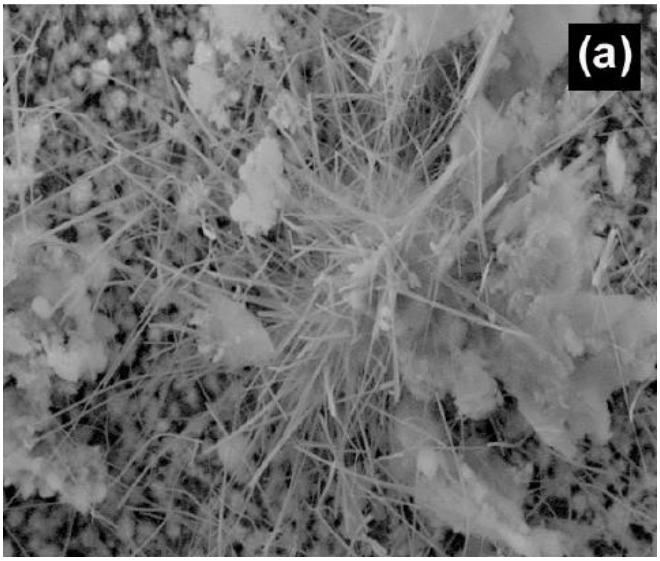


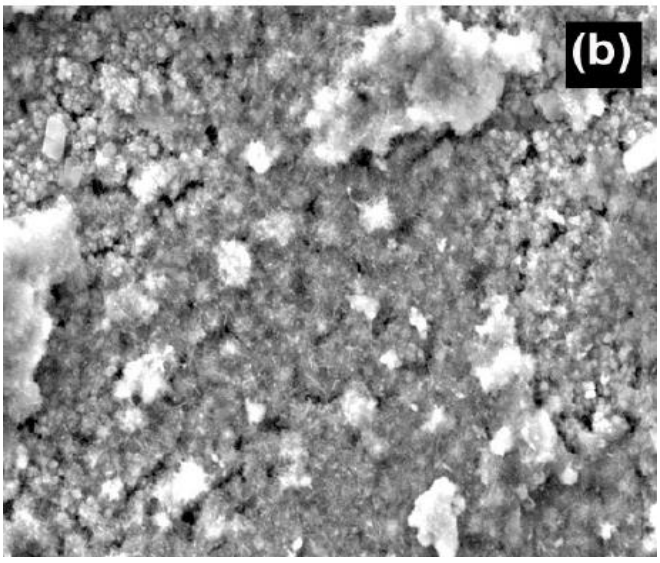


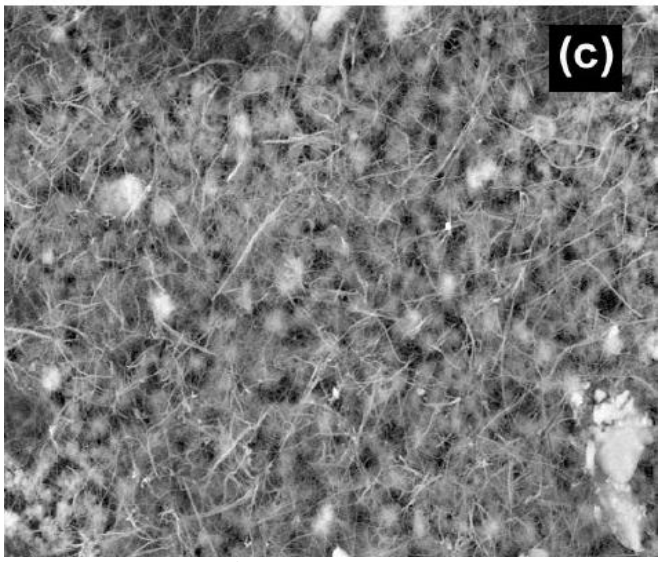


**Fig. 17 SEM images of (a) ZnO, (b) ZnMnO, and (c) ZnMgO [49]**

The substrate materials for the Atomic Layer Deposition (ALD) method used to deposit thin $SnO_2$ films were the $MgCa_2Zn$ and $MgCa_2ZnGd_3$ alloys [50]. Because magnesium and its alloys are biocompatible and biodegradable, they make appealing temporary implants. Additionally, magnesium has favorable osteoinductive and mechanical qualities. The $SnO_2$ films' lamellar-like shape and heterogeneous structure, which are made of bundles of nanorods. Shorter and thicker $SnO_2$ crystallites are formed when the ALD deposition time is extended. Every surface had visible pores and was rough. Furthermore, as the $SnO_2$ film's thickness rose, the lamellae got thicker. EDX studies highlighted that tin content will be increased when the thickness was increased. While less tin content was observed in the absence of gadolinium.

## 4. Conclusion

Preparation of metal sulphide, metal oxide, metal selenide and metal telluride films could be carried out using different deposition methods. Morphology of the prepared films will be studied using scanning electron microscope technique. When the electrons in the films interacted with the atoms, they produced signals that revealed crucial details about the crystalline structure, texture, and chemical composition. Data were gathered (in a specific sample area) and two-dimensional (black and white) images were generated. Based on the literature, experimental conditions will determine the properties and quality of films.

## Funding Statement

Author (Ho SM) was financially supported by INTI International University, Malaysia.

## Acknowledgments

This research work (Ho SM) was financially supported by INTI International University.

## References


[1] T.M. Razykov et al., "Solar Photovoltaic Electricity: Current Status and Future Prospects," *Solar Energy*, vol. 85, no. 8, pp. 1580-1608, 2011. [CrossRef] [Google Scholar] [Publisher Link]

[2] Martin A. Green et al., "Solar Cell Efficiency Tables (Version 62)," *Progress in Photovoltaics*, vol. 31, no. 7, pp. 651-663, 2023. [CrossRef] [Google Scholar] [Publisher Link]

[3] Issei Suzuki et al., "Low-Temperature Growth of $BaZrO_3$ and $Ba(Zr,Y)O_{3-\delta}$ Thin Films Via Spray Pyrolysis Deposition," *Thin Solid Films*, vol. 792, pp. 1-11, 2024. [CrossRef] [Google Scholar] [Publisher Link]

[4] Joana Moreira, A. Catarina Vale, and Natalia M. Alves, "Spin-Coated Freestanding Films for Biomedical Applications," *Journal of Materials Chemistry B*, vol. 9, no. 18, pp. 3778-3799, 2021. [CrossRef] [Google Scholar] [Publisher Link]

[5] Ghazi Aman Nowsherwan et al., "Numerical Optimization and Performance Evaluation of ZnPC:PC70BM Based Dye-Sensitized Solar Cell," *Scientific Reports*, vol. 13, no. 1, pp. 1-16, 2023. [CrossRef] [Google Scholar] [Publisher Link]

[6] A.J. Santos et al., "Application of Advanced (S)TEM Methods for the Study of Nanostructured Porous Functional Surfaces: A Few Working Examples," *Materials Characterization*, vol. 185, pp. 1-15, 2022. [CrossRef] [Google Scholar] [Publisher Link]

[7] Audrius Drabavicius et al., "Photoelectrochemical, Raman Spectroscopy, XRD and Photoluminescence Study of Disorder in Electrochemically Deposited Kesterite Thin Film," *Journal of Alloys and Compounds*, vol. 842, 2020. [CrossRef] [Google Scholar] [Publisher Link]

[8] Kalliopi Mavridou et al., "Oxidation of $Cu_3N$ Thin Films Obtained from Cu Annealed Under $NH_3$:$O_2$ Flow: A Raman and N-K-Edge NEXAFS Study," *Journal of Alloys and Compounds*, vol. 914, 2022. [CrossRef] [Google Scholar] [Publisher Link]

[9] Kristina Cajko et al., "Influence of Different Metal Concentrations on the Morphology of Ag-$As_2Ch_3$ Thin Films Analyzed by Rutherford Backscattering Spectrometry and Energy Dispersive Spectroscopy," *Applied Surface Science*, vol. 510, 2020. [CrossRef] [Google Scholar] [Publisher Link]

[10] Hyeon-Gyu Min, and Jun-Hyub Park, "Real-Time Dynamic Behavior Analysis of Thin Film During in-situ SEM Tensile Testing," *Heliyon*, vol. 10, no. 4, pp. 1-8, 2024. [CrossRef] [Google Scholar] [Publisher Link]

[11] Feyza Guzelcimen et al., "The Effect of Thickness on Surface Structure of rf Sputtered $TiO_2$ Thin Films by XPS, SEM/EDS, AFM and SAM," *Vacuum*, vol. 182, 2020. [CrossRef] [Google Scholar] [Publisher Link]

[12] Atsutaka Kato et al., "XPS and SEM Analysis between Li/$Li_3PS_4$ Interface with Au Thin Film for All-Solid-State Lithium Batteries," *Solid State Ionics*, vol. 322, pp. 1-4, 2018. [CrossRef] [Google Scholar] [Publisher Link]

[13] Esmaiel Nouri et al., "A Comparative Study of Heat Treatment Temperature Influence on the Thickness of Zirconia Sol-Gel Thin Films by Three Different Techniques: SWE, SEM and AFM," *Surface and Coatings Technology*, vol. 206, no. 19-20, pp. 3809-3815, 2012. [CrossRef] [Google Scholar] [Publisher Link]

[14] A. Balakrishna, M.M. Duvenhage, and H.C. Swart, "Surface and Chemical Characterization of ZnO:$Eu^{3+}$/$Yb^{3+}$ Spin Coated Thin Films Using SEM-CL and TOF-SIMS," *Vacuum*, vol. 157, pp. 376-383, 2018. [CrossRef] [Google Scholar] [Publisher Link]

[15] Gayan W.C. Kumarage et al., "Enhancing the Photovoltaic Performance of $Cd_{(1-x)}Zn_xS$ Thin Films Using Seed Assistance and EDTA Treatment," *Micro*, vol. 3, no. 4, pp. 867-878, 2023. [CrossRef] [Google Scholar] [Publisher Link]

[16] Elham Karimizand et al., "Study of the Optimal Conditions and Mechanism of CdS Thin Layers Formation by Chemical Bath Deposition Method," *Asian Journal of Chemistry*, vol. 25, no. 3, pp. 1701-1705, 2013. [CrossRef] [Google Scholar] [Publisher Link]

[17] Noyoung Yoon et al., "Recent Advances in CuInS2-Based Photocathodes for Photoelectrochemical H2 Evolution," *Nanomaterials*, vol. 13, no. 8, pp. 1-17, 2023. [CrossRef] [Google Scholar] [Publisher Link]

[18] E. Anuja, and R. Thiruneelakandan, "Fabrication, Structural, Optical, Electrical Properties and Influence of Complexing Agents on Ternary CuZnS2 Thin Film," *Asian Journal of Chemistry*, vol. 33, no. 11, pp. 2762-2766, 2021. [CrossRef] [Publisher Link]

[19] S.S. Tulenin et al., "Synthesis and Characterization of Chemical Bath Deposited Lead Sulfide Thin Films in Ultrasound and Microwave Irradiation," *Asian Journal of Chemistry*, vol. 30, no. 7, pp. 1655-1658, 2018. [CrossRef] [Google Scholar] [Publisher Link]

[20] Marcelo Augusto Malagutti et al., "Optimizing CuFeS2 Chalcopyrite Thin Film Synthesis: A Comprehensive Three-Step Approach Using Ball-Milling, Thermal Evaporation, and Sulfurization Applied for Thermoelectric Generation," *Applied Sciences*, vol. 13, no. 18, pp. 1-17, 2023. [CrossRef] [Google Scholar] [Publisher Link]

[21] Raghad Y. Mohammed, "Annealing Effect on the Structure and Optical Properties of CBD-ZnS Thin Films for Windscreen Coating," *Materials*, vol. 14, no. 22, pp. 1-11, 2021. [CrossRef] [Google Scholar] [Publisher Link]

[22] Ogah E. Ogah et al., "Thin films of Tin Sulphide for Use in Thin Film Solar Cell Devices," *Thin Solid Films*, vol. 517, no. 7, pp. 2485-2488, 2009. [CrossRef] [Google Scholar] [Publisher Link]

[23] Maxim Ganchev et al., "Rapid Thermal Processing of Kesterite Thin Films," *Coatings*, vol. 13, no. 8, pp. 1-14, 2023. [CrossRef] [Google Scholar] [Publisher Link]

[24] Vu Minh Han Cao et al., "Fabrication of the $Cu_2ZnSnS_4$ Thin Film Solar Cell via a Photo-Sintering Technique," *Applied Sciences*, vol. 12, no. 1, pp. 1-9, 2021. [CrossRef] [Google Scholar] [Publisher Link]

[25] Liangliang Yang et al., "Thermoelectric Properties of Cu2Se Nano-Thin Film by Magnetron Sputtering," *Materials*, vol. 14, no. 8, pp. 1-13, 2021. [CrossRef] [Google Scholar] [Publisher Link]
[26] Sung-Tae Kim et al., "CuInSe2-Based Near-Infrared Photodetector," *Applied Sciences*, vol. 12, no. 1, pp. 1-7, 2022. [CrossRef] [Google Scholar] [Publisher Link]
[27] Ovidiu Toma et al., "Effect of RF Power on the Physical Properties of Sputtered ZnSe Nanostructured Thin Films for Photovoltaic Applications," *Nanomaterials*, vol. 11, no. 11, pp. 1-15, 2021. [CrossRef] [Google Scholar] [Publisher Link]
[28] R.M. Ovhal, A.H. Manikshete, and S.G. Holikatti, "Synthesis and Characterization of Cadmium Selenide Thin Films," *Asian Journal of Chemistry*, vol. 23, no. 7, pp. 2973-2976, 2011. [Google Scholar] [Publisher Link]
[29] P.P. Hankare et al., "Synthesis and Characterization of Nickel Selenide Thin Films Deposited by Chemical Method," *Journal of Alloys and Compounds*, vol. 490, no. 1-2, pp. 228-231, 2010. [CrossRef] [Google Scholar] [Publisher Link]
[30] R. Divya, N. Manikandan, and G. Vinitha, "Synthesis and Characterization of Nickel Doped Zinc Selenide Nanospheres for Nonlinear Optical Applications," *Journal of Alloys and Compounds*, vol. 791, pp. 601-612, 2019. [CrossRef] [Google Scholar] [Publisher Link]
[31] Zulkarnain Zainal et al., "Electrodeposition of tin Selenide Thin Film Semiconductor: Effect of The Electrolytes Concentration on the Film Properties," *Solar Energy Materials and Solar Cells*, vol. 79, no. 2, pp. 125-132, 2003. [CrossRef] [Google Scholar] [Publisher Link]
[32] Remigijus Ivanauskas et al., "Impact of Surface Morphology and Thickness of Tin Selenide Thin Films on their Optical Properties," *Surfaces and Interfaces*, vol. 28, 2022. [CrossRef] [Google Scholar] [Publisher Link]
[33] A.U. Ubale et al., "Characterization of Nanostructured Iron Selenide Thin Films Grown by Chemical Route at Room Temperature," *Materials Research Bulletin*, vol. 48, no. 2, pp. 863-868, 2013. [CrossRef] [Google Scholar] [Publisher Link]
[34] Z. Qin et al., "Flower-Like Pyrite FeSe2 Nanoparticles with Enhanced Optical Properties by Hot-Injection," *Vacuum*, vol. 111, pp. 157-159, 2015. [CrossRef] [Google Scholar] [Publisher Link]
[35] Chia-Hua Huang et al., "Deposition Technologies of High-Efficiency CIGS Solar Cells: Development of Two-Step and Co-Evaporation Processes," *Crystals*, vol. 8, no. 7, pp. 1-17, 2018. [CrossRef] [Google Scholar] [Publisher Link]
[36] Jun Ling et al., "Electrodeposition of CdTe Thin Films for Solar Energy Water Splitting," *Materials*, vol. 13, no. 7, pp. 1-9, 2020. [CrossRef] [Google Scholar] [Publisher Link]
[37] Nor A. Abdul-Manaf et al., "Electro-Plating and Characterisation of CdTe Thin Films Using CdCl2 as the Cadmium Source," *Energies*, vol. 8, no. 10, pp. 10883-10903, 2015. [CrossRef] [Google Scholar] [Publisher Link]
[38] Kisan C. Rathod et al., "Growth Mechanism, Structural and Photoelectrochemical Study of Zinc Tellurium Thin Film," *Asian Journal of Chemistry*, vol. 34, no. 3, pp. 715-719, 2022. [CrossRef] [Google Scholar] [Publisher Link]
[39] Chunmin Liu et al., "Ta Doping E_Ect on Structural and Optical Properties of InTe Thin Films," *Nanomaterials*, vol. 10, no. 9, pp. 1-13, 2020. [CrossRef] [Google Scholar] [Publisher Link]
[40] M. Boustani et al., "Characterization of CuInTe2 Thin Films Prepared by Flash Evaporation," *Semiconductor Science and Technology*, vol. 12, no. 12, pp. 1658-1661, 1997. [CrossRef] [Google Scholar] [Publisher Link]
[41] A.S. Meshram, Y.D. Tembhurkar, and O.P. Chimankar, "Structural, Optical and Electrical Properties of CuInTe2 Thin Films Prepared by Spray Pyrolysis," *International Journal of Advance Research in Science and Engineering*, vol. 6, no. 6, pp. 1735-1745, 2017. [Google Scholar] [Publisher Link]
[42] P. Muthusamy, and A. Panneerselvam, "Optical Constants of Brush Electrodeposited CuInTe2 Films," *Chalcogenide Letters*, vol. 16, no. 5, pp. 249-255, 2019. [Google Scholar] [Publisher Link]
[43] T. Mahalingam et al., "Studies on Electroplated Copper Indium Telluride Thin Films," *Journal of New Materials for Electrochemical Systems*, vol. 13, no. 1, pp. 77-82, 2010. [Google Scholar] [Publisher Link]
[44] Abdul Ghaffar, Iftikhar Ahmed Channa, and Ali Dad Chandio, "Mitigating UV-Induced Degradation in Solar Panels through ZnO Nanocomposite Coatings," *Sustainability*, vol. 16, no. 15, pp. 1-16, 2024. [CrossRef] [Google Scholar] [Publisher Link]
[45] Ling Xu et al., "Preparation of CuO Thin Film with Corncob-Like Morphology *via* Chemical Solution Processing," *Asian Journal of Chemistry*, vol. 23, no. 5, pp. 2295-2298, 2011. [Google Scholar] [Publisher Link]
[46] S. Morkoc Karadeniz et al., "Properties of NiO Thin Films Prepared by Chemical Spray Pyrolysis Using NiSO4 Precursor Solution," *Asian Journal of Chemistry*, vol. 24, pp. 1765-1768, 2012. [Google Scholar] [Publisher Link]
[47] S.K. Jasmin, K. Mohanraj, and R.P. Jebin, "Spray Deposited Ni Doped Co3O4 Thin Films for Electrochemical Applications," *Asian Journal of Chemistry*, vol. 35, no. 1, pp. 239-246, 2023. [CrossRef] [Publisher Link]
[48] Guven Turgut, Demet Tatar, and Bahattin Duzgun, "Relationship Between the Doping Levels and Some Physical Properties of SnO2:Sb Thin Films Spray-Deposited on Optical Glass," *Asian Journal of Chemistry*, vol. 25, no. 1, pp. 245-250, 2013. [CrossRef] [Google Scholar] [Publisher Link]
[49] K. Radhi Devi et al., "Micro-structural, Morphological and Optical Properties of Pure and Metal (Mn & Mg) Doped ZnO Thin Films by Low Cost SILAR Method," *Asian Journal of Chemistry*, vol. 31, no. 4, pp. 901-906, 2019. [CrossRef] [Publisher Link]
[50] Aneta Kania et al., "Structure and Selected Properties of $SnO_2$ Thin Films," *Materials*, vol. 17, no. 13, pp. 1-16, 2024. [CrossRef] [Google Scholar] [Publisher Link]